Fault-Tolerant Multiqubit Geometric Entangling Gates Using Photonic Cat-State Qubits

Ye-Hong Chen, Roberto Stassi, Wei Qin, Adam Miranowicz, and Franco Nori

Phys. Rev. Applied **18**, 024076 — Published 29 August 2022

DOI: 10.1103/PhysRevApplied.18.024076

Fault-tolerant multiqubit geometric entangling gates using photonic cat-state qubits

Ye-Hong Chen,[1,2] Roberto Stassi,[1,3] Wei Qin,[1] Adam Miranowicz,[1,4] and Franco Nori[1,2,5]

[1] *Theoretical Quantum Physics Laboratory, RIKEN Cluster for Pioneering Research, Wako-shi, Saitama 351-0198, Japan*
[2] *RIKEN Center for Quantum Computing (RQC), Wako-shi, Saitama 351-0198, Japan*
[3] *Dipartimento di Scienze Matematiche e Informatiche, Scienze Fisiche e Scienze della Terra, Università di Messina, 98166, Messina, Italy*
[4] *Institute of Spintronics and Quantum Information, Faculty of Physics, Adam Mickiewicz University, 61-614 Poznań, Poland*
[5] *Department of Physics, University of Michigan, Ann Arbor, Michigan 48109-1040, USA*

(Dated: August 11, 2022)

We propose a theoretical protocol to implement multiqubit geometric gates (i.e., the Mølmer-Sørensen gate) using photonic cat-state qubits. These cat-state qubits stored in high-Q resonators are promising for hardware-efficient universal quantum computing. Specifically, in the limit of strong two-photon drivings, phase-flip errors of the cat-state qubits are effectively suppressed, leaving only a bit-flip error to be corrected. Because this dominant error commutes with the evolution operator, our protocol preserves the error bias, and, thus, can lower the code-capacity threshold for error correction. A geometric evolution guarantees the robustness of the protocol against stochastic noise along the evolution path. Moreover, by changing detunings of the cavity-cavity couplings at a proper time, the protocol can be robust against parameter imperfections (e.g., the total evolution time) without introducing extra noises into the system. As a result, the gate can produce multi-mode entangled cat states in a short time with high fidelities.

Keywords: Cat-state qubit; Geometric gate; Parametric driving

I. INTRODUCTION

Quantum computers promise to drastically outperform classical computers on certain problems, such as factoring and unstructured database searching [1–5]. Recent experiments with superconducting qubits [6] and photons [7] have already demonstrated quantum advantage. To perform useful large-scale quantum computation, fragile quantum states must be protected from errors, which arise due to their inevitable interaction with the environment [1–3]. Aiming at this problem, strategies for quantum error correction have been being developed in the past decades [5, 8–26]. For instance, because most noisy environments are only locally correlated, quantum information can be protected by employing non-locality using, e.g., entangled qubit states [8], spatial distance [10], and their combinations [22, 26]. Note that this strategy has been extended to states that are non-local in the phase space of an oscillator [5, 11–18, 27–35], such as Schrödinger cat states [17, 18, 36–43]. Encoding quantum information in such bosonic states has the benefit of involving fewer physical components. In particular, cat-state qubits (which are formed by even and odd coherent states of a single optical mode) are promising for hardware-efficient universal quantum computing because these cat-state qubits are noise-biased [15, 16]. This kind of logical qubit experiences only bit-flip noise, while the phase-flip errors are exponentially suppressed. Additional layers of error correction can focus only on the bit-flip error, so that the number of building blocks can be significantly reduced [11, 25, 44].

In this manuscript, we propose to use Kerr cat-state qubits to implement multiqubit geometric gates, i.e., the well-known Mølmer-Sørensen (MS) entangling gate [45, 46] and its multiqubit generalizations [47]. Generally, the MS gate is a two-qubit geometric gate possessing a built-in noise-resilience feature against certain types of local noises [48–54]. It is also a significant resource for Grover's quantum search algorithm [3, 55] without a third ancilla bit [56].

Previous works [57–66] implementing the MS gate using physical qubits (such as trapped ions and atoms) may experience various errors including bit flips, phase flips, qubit dephasing, etc. Thus, a huge physical resource is needed to correct the various errors [59, 67–69]. This requirement has driven researchers to optimize such implementations with respect to speed and robustness to nonideal control environments using extra control fields [63–66]. However, additional control fields may induce extra noises which should be corrected by using additional physical resources. All the above factors impede in scaling up the number of qubits because error channels increase when the number of physical qubits increases.

Instead, Kerr cat-state qubits, which experience only a bit-flip error, can be an excellent choice to overcome the above problems. This is because the dominant error commutes with the MS gate matrix. As a result, an erroneous gate operation is equivalent to an error-free gate followed by an error, i.e., our cat-code gates preserve the error bias. The code capacity threshold for error correction using such biased-noise qubits is higher than that using qubits without such structured noise [44, 70]. We suggest, using cavity and circuit quantum electrodynamics [25, 41, 71], to realize our protocol. This can avoid some problems in trapped-ion implementations, such as the limitation of a Lamb-Dicke parameter. Note that the MS entangling gate was

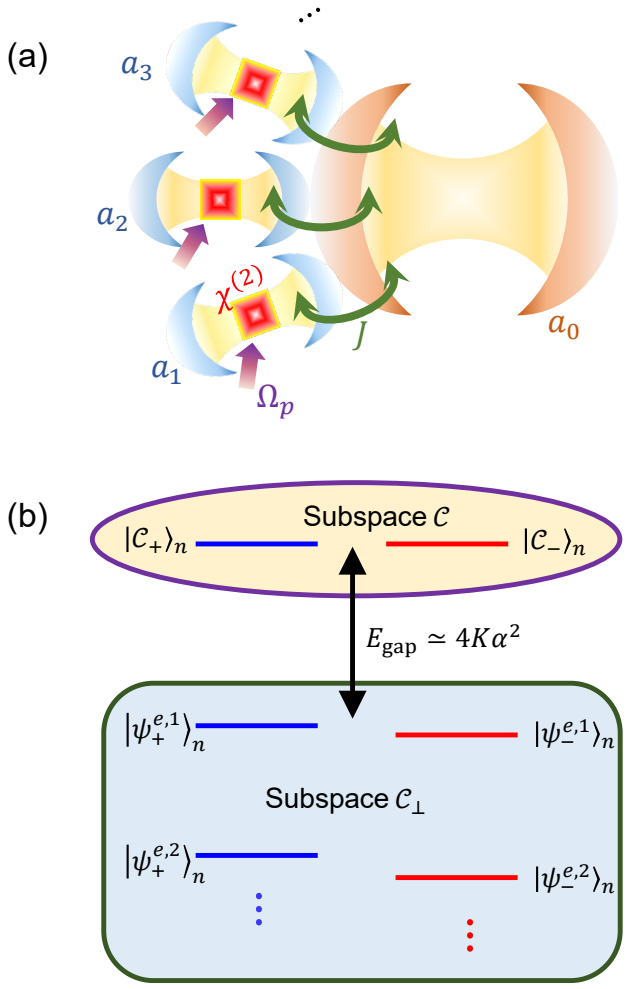

FIG. 1. (a) Schematic of N Kerr-nonlinear resonators coupled to another resonator. Driving the $\chi^{(2)}$ nonlinearity induces a two-photon driving in the cavity mode a_n. (b) Eigenspectrum of the nth Kerr parametric oscillator, $H_n^{\rm Kerr}$, in the rotating frame determined by Eq. (4). The excited states appear at a lower energy because the Kerr nonlinearity is negative.

initially proposed [45, 46] and experimentally realized [57] in trapped-ion systems.

II. MODEL AND EFFECTIVE HAMILTONIAN

We consider N Kerr-nonlinear resonators (a_1, a_2, …, a_N) with the same frequency ω_c, which are simultaneously coupled to another resonator (a_0) with frequency ω_0 [See Fig. 1(a)]. The interaction Hamiltonian is

$$H_{\rm int} = \sum_{n=1}^{N} J a_n a_0^\dagger \exp\left(i\Delta t\right) + \text{h.c.}, \tag{1}$$

where J is the intercavity coupling strength and $\Delta = \omega_0 - \omega_c$ is the detuning. Hereafter, we assume $\hbar = 1$. Each Kerr-nonlinear resonator is resonantly driven by a two-photon drive of frequency $\omega_p = 2\omega_c$ and amplitude Ω_p [25, 71]. The total Hamiltonian of the system in the interaction picture reads

$$\begin{aligned} H &= \sum_{n=1}^{N} H_n^{\rm Kerr} + H_{\rm int}, \\ H_n^{\rm Kerr} &= -K a_n^{\dagger 2} a_n^2 + \left(\Omega_p a_n^2 + \text{h.c.}\right), \end{aligned} \tag{2}$$

where $H_n^{\rm Kerr}$ describes Kerr parametric oscillators (KPOs) with Kerr nonlinearity K [72, 73].

To understand the Hamiltonian $H_n^{\rm Kerr}$ in Eq. (2), following Refs. [15, 16, 25, 70, 71], we can apply the displacement transformation

$$D_n(\pm\alpha) = \exp\left[\pm\alpha\left(a_n^\dagger - a_n\right)\right], \tag{3}$$

so that Eq. (2) becomes

$$\begin{aligned} H_n' =& D_n(\pm\alpha) H_n^{\rm Kerr} D_n^\dagger(\pm\alpha) \\ =& -K\left[4\alpha^2 a_n^\dagger a_n - a_n^{\dagger 2} a_n^2 \mp 2\alpha(a_n^{\dagger 2} a_n + \text{h.c.})\right]. \end{aligned} \tag{4}$$

Hereafter, we choose $\{K, \Omega_p, J, \Delta\} > 0$ for simplicity, then, $\alpha = \alpha^* > 0$. Because of $H_n'|\nu = 0\rangle = 0$, the vacuum state $|0\rangle$ is exactly an eigenstate of H_n'. Therefore, the coherent states $|\pm\alpha\rangle$, or, equivalently, their superpositions

$$|\mathcal{C}_\pm\rangle_n = \mathcal{N}_\pm\left[D_n(\alpha) \pm D_n(-\alpha)\right]|0\rangle_n, \tag{5}$$

are the eigenstates of $H_n^{\rm Kerr}$ in the original frame. Here, $\mathcal{N}_\pm$ are normalization coefficients. In the limit of large α, $\alpha^2 \gg \alpha^1, \alpha^0$, Eq. (4) is approximated by

$$H_n' \simeq -4K\alpha^2 a_n^\dagger a_n, \tag{6}$$

which is the Hamiltonian of a (inverted) harmonic oscillator [25]. Thus, in the original frame, the eigenspectrum of $H_n^{\rm Kerr}$ can be divided into an even- and odd-parity manifolds as shown in Fig. 1(b). The excited states appear at a lower energy because the Kerr nonlinearity is negative. In the limit of large α, we can approximatively express the first-excited states as the two orthogonal states

$$|\psi_\pm^{e,1}\rangle_n = \mathcal{N}_e^\pm\left[D_n(\alpha) \mp D_n(-\alpha)\right]|\nu = 1\rangle_n, \tag{7}$$

which are the even- and odd-parity states, respectively. Here, $\mathcal{N}_e^\pm$ are normalization coefficients.

As shown in Fig. 1(b), the orthogonal cat states $|\mathcal{C}_\pm\rangle_n$ can span a cat subspace $\mathcal{C}$, which is separated from the excited eigenstates of KPO by an energy gap $E_{\rm gap} \simeq 4K\alpha^2$ (i.e., the energy gap between $|\mathcal{C}_\pm\rangle_n$ and $|\psi_\pm^{e,1}\rangle_n$). In the limit of large α, the action of a_n only flips the two cat states, i.e.,

$$a_n|\mathcal{C}_\pm\rangle_n \simeq \alpha|\mathcal{C}_\mp\rangle_n. \tag{8}$$

The action of $a_n^\dagger$ on a state in the cat subspace causes transitions to the excited states, i.e.,

$$a_n^\dagger|\mathcal{C}_\pm\rangle_n \to \alpha|\mathcal{C}_\mp\rangle_n + |\psi_\mp^{e,1}\rangle_n. \tag{9}$$

When the KPOs are coupled to the cavity mode a_0, with the interaction Hamiltonian $H_{\rm int}$, the Hamiltonian describing transitions to the excited states (projected onto the eigenstates of $H_n^{\rm Kerr}$) is

$$H_e = \sum_{n=1}^{N} \frac{E_{\rm gap}}{2}(|\mathcal{C}_\pm\rangle_n\langle\mathcal{C}_\pm| - |\psi_\pm^{e,1}\rangle_n\langle\psi_\pm^{e,1}|) + J\left[|\psi_\mp^{e,1}\rangle_n\langle\mathcal{C}_\pm|a_0\exp(-i\Delta t) + \text{h.c.}\right]. \quad (10)$$

Here, we have defined and used the projection operator

$$P_{\rm KPO} = \sum_{n=1}^{N}\left(|\mathcal{C}_\pm\rangle_n\langle\mathcal{C}_\pm| + \sum_{\nu=1}^{\infty}|\psi_\pm^{e,\nu}\rangle_n\langle\psi_\pm^{e,\nu}|\right). \quad (11)$$

Because $E_{\rm gap} > 0$, according to Eq. (10), the probability of excitation to the states $|\psi_\pm^{e,1}\rangle_n$ is suppressed by

$$P_e \sim \frac{NJ^2}{(E_{\rm gap}+\Delta)^2}, \quad (12)$$

which is proportional to both, the number N of cat-state qubits and the square of the coupling strength J. Therefore, in the limit of $J \ll E_{\rm gap}$, the excited eigenstates of the KPOs remain unpopulated. Then, the dynamics of the system is restricted in the cat subspace with an effective Hamiltonian

$$H_{\rm eff} \simeq \sum_{n=1}^{N}\frac{\Omega_p^2}{K}(|\mathcal{C}_-\rangle_n\langle\mathcal{C}_-| + |\mathcal{C}_+\rangle_n\langle\mathcal{C}_+|) + J\alpha\left[|\mathcal{C}_+\rangle_n\langle\mathcal{C}_-|\left(a_0e^{-i\Delta t} + a_0^\dagger e^{i\Delta t}\right) + \text{h.c.}\right].$$

Here, the first-line expression in $H_{\rm eff}$ can be dropped because it is proportional to the identity matrix $\mathbb{1}_n = |\mathcal{C}_-\rangle_n\langle\mathcal{C}_-| + |\mathcal{C}_+\rangle_n\langle\mathcal{C}_+|$ in the dressed-state subspace. In the limit of large α, by using the definition of Pauli matrices $\sigma_n^+ = |\mathcal{C}_-\rangle_n\langle\mathcal{C}_+|$ and $\sigma_n^- = (\sigma_n^+)^\dagger$, $H_{\rm eff}$ becomes

$$\begin{aligned} H_{\rm eff} \simeq& J\alpha\sum_{n=1}^{N}\left[(\sigma_n^+ + \sigma_n^-)\left(a_0e^{-i\Delta t} + a_0^\dagger e^{i\Delta t}\right)\right] \\ =& 2J\alpha S_x\left(a_0e^{-i\Delta t} + a_0^\dagger e^{i\Delta t}\right), \end{aligned} \quad (13)$$

where $S_x = \frac{1}{2}\sum_n(\sigma_n^+ + \sigma_n^-)$.

III. IMPLEMENTING THE MS GATES

The integral of $H_{\rm eff}$ can be calculated exactly [46],

$$U_{\rm MS}(t) = \exp\left\{-i\left[\chi(t)a_0^\dagger S_x + \text{h.c.}\right]\right\}\exp\left[-i\beta(t)S_x^2\right],$$

where

$$\begin{aligned} \chi(t) =& \frac{2iJ\alpha}{\Delta}\left[1-\exp(i\Delta t)\right], \\ \beta(t) =& \left(\frac{2J\alpha}{\Delta}\right)^2(\sin\Delta t - \Delta t). \end{aligned} \quad (14)$$

One observes that in the phase space determined by the cavity mode a_0, $\chi(t)$ draws m circles with a radius $r = 2J\alpha/\Delta$ and a rotation angle $\theta = \Delta t_g$ when

$$t = t_g = \frac{2m\pi}{\Delta}. \quad (m = 1, 2, \ldots) \quad (15)$$

Here, t_g is the gate time. Thus, the cavity mode a_0 evolves along a circle in phase space and returns to its (arbitrary) initial state after m periods. Meanwhile, $\beta(t_g)$ can be expressed by the area A enclosed by $\chi(t)$ as

$$\beta(t_g) = -2m\pi r^2 = -2mA, \quad (16)$$

which is a geometric phase. The evolution operator at the time $t = t_g$ reads

$$U_{\rm MS}(t_g) = \exp\left[-i\beta(t_g)S_x^2\right]. \quad (17)$$

In particular, when $\beta(t_g) = -\pi/2$ and N is even, $U_{\rm MS}(t_g)$ accomplishes the transformations:

$$\bigotimes_{n=1}^{N}|\mathcal{C}_\pm\rangle_n \xrightarrow{U_{\rm MS}(t_g)} \frac{1}{\sqrt{2}}\left(\bigotimes_{n=1}^{N}|\mathcal{C}_\pm\rangle_n + i\bigotimes_{n=1}^{N}|\mathcal{C}_\mp\rangle_n\right),$$

which maps product states (i.e., the input state $|\psi_{\rm in}\rangle$) into maximally entangled cat states (i.e., the output state $|\psi_{\rm out}\rangle$). Accompanied by single-qubit rotations [74–77], the MS gate can be applied in Grover's quantum search algorithm for both the marking and state amplification steps [56, 78]. A possible approach for such single-qubit gates is shown in the Appendix A. The generation of input states in a KPO has been experimentally realized [74]. For instance, using time-dependent two-photon drivings, a cat state with a fidelity $\gtrsim 95\%$ [71] in the presence of decoherence can be generated. For clarity, in the Appendix B, we describe a possible protocol to generate the cat states. Hereafter, we use QuTip [79, 80] for numerical simulations.

The average fidelity of an N-qubit gate over all possible initial states is defined by [82, 83]

$$\begin{aligned} \bar{F}_N =& \frac{\text{Tr}(MM^\dagger) + |\text{Tr}(M)|^2}{D^2+D}, \\ M =& \mathcal{P}_c U_{\rm MS}^\dagger U(t_g)\mathcal{P}_c. \end{aligned} \quad (18)$$

Here, $\mathcal{P}_c$ (D) is the projector (dimension) of the computing subspace, and

$$U(t_g) = \exp(-iHt_g) \quad (19)$$

is the actual evolution operator of the system calculated from the total Hamiltonian H. If no otherwise specified, the numerical simulations in our manuscript are carried out using the full Schrödinger equation (for coherent dynamics) and the full Lindblad master equation (for incoherent dynamics) with the full Hamiltonian H in Eq. (2) in the entire space.

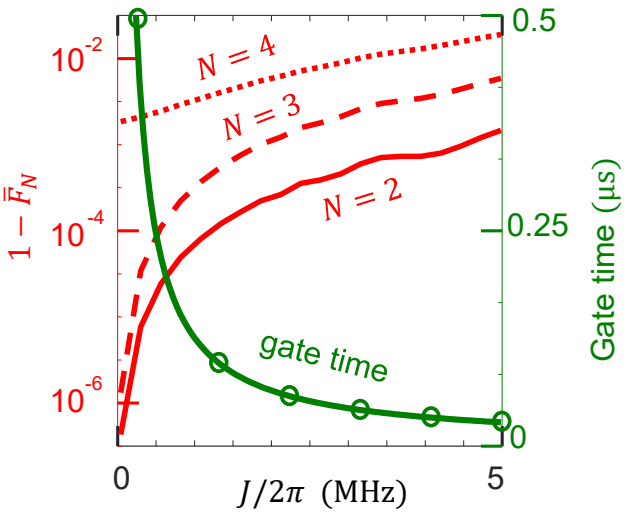

FIG. 2. Gate infidelities $(1-\bar{F}_N)$ and gate time $t_g = \pi/(2J\alpha)$ (i.e., $m = 1$) calculated for the total Hamiltonian H, for different values of the coupling strength J. Here, the gate fidelity $\bar{F}_N$ is defined in Eq. (18). We assume a realistic Kerr nonlinearity $K/2\pi = 5$ MHz [81]. For $\beta(t_g) = -\pi/2$, we choose other parameters $\Delta = 4J\alpha$ [i.e., $m = 1$ in Eq. (20)] and $\alpha = 2$.

Current experiments using superconducting systems [40, 74, 81, 84, 85] have achieved a driving amplitude $\Omega_p/2\pi \sim 10$–40 MHz and a Kerr nonlinearity $K/2\pi \sim 1$–10 MHz. Hereafter, we choose $K/2\pi = 5$ MHz. Note that Δ and J should obey

$$\Delta = 4\sqrt{m}J\alpha, \tag{20}$$

for $\beta(t_g) = -\pi/2$. Therefore, the gate time

$$t_g = \frac{\pi\sqrt{m}}{2J\alpha} \tag{21}$$

is inversely proportional to J [see the green-solid curve with circles in Fig. 2]. The gate infidelities $(1-\bar{F}_N)$ for $N = 2$, 3, 4 versus J are shown in Fig. 2. When $J/2\pi \lesssim 0.5$ MHz, we can achieve high-fidelity $\bar{F}_N \gtrsim 99.9\%$ multiqubit gates within a gate time $t_g \lesssim 500$ ns.

IV. ANALYSIS OF DECOHERENCE

For the resonators, we consider two kinds of noise: single-photon loss and pure dephasing. The system dynamics is described by the Lindblad master equation

$$\dot{\rho} = -i[H,\rho] + \sum_{j=0}^{N} \kappa_j \mathcal{D}[a_j]\rho + \gamma_j \mathcal{D}[a_j^\dagger a_j]\rho, \tag{22}$$

where $\mathcal{D}[o]\rho = o\rho o^\dagger - \left(o^\dagger o\rho + \rho o^\dagger o\right)/2$ is the standard Lindblad superoperator and κ_j (γ_j) is the single-photon loss (pure dephasing) rate of the jth cavity mode. Without loss of generality, for the KPOs, we assume $\kappa_n = \kappa$ and $\gamma_n = \gamma$ ($n = 1, 2, \ldots, N$). Note that the influence of decoherence in the cavity mode a_0 is different from that in the KPOs. We initially consider only decoherence in the cavity mode a_0 i.e., assuming $\kappa_n = \gamma_n = 0$. For simplicity, we choose an initial state

$$|\psi_{\rm in}\rangle = |0\rangle_0 \bigotimes_{n=1}^{N} |\mathcal{C}_+\rangle_n. \tag{23}$$

The fidelity

$$F_{\rm out} = \langle\psi_{\rm out}|\rho(t_g)|\psi_{\rm out}\rangle, \tag{24}$$

of the output state vs decoherence in the cavity mode a_0 is shown in Fig. 3(a). We find that the system is mostly insensitive to the decoherence of the cavity mode a_0 because it can be adiabatically eliminated for large Δ.

For a clear understanding of the influence of decoherence in the KPOs, we can project the system onto the eigenstates of $H_n^{\rm Kerr}$ [15, 16, 25, 70, 71, 86, 87]. Then the master equation becomes

$$\begin{aligned}\dot{\rho} \simeq & -i[P_{\rm KPO}HP_{\rm KPO},\rho] + \kappa_0\mathcal{D}[a_0]\rho + \gamma_0\mathcal{D}[a_0^\dagger a_0]\rho \\ & + \sum_{n=1}^{N} \kappa_n \mathcal{D}[P_{\rm KPO}a_n P_{\rm KPO}]\rho \\ & + \gamma_n \mathcal{D}[P_{\rm KPO}a_n^\dagger a_n P_{\rm KPO}]\rho. \end{aligned} \tag{25}$$

A. Single-photon loss in the Kerr parametric oscillators

When γ_n and κ_n are much smaller than the energy gap $E_{\rm gap}$, the dynamics of the cat-state qubits is still well confined to the subspace $\mathcal{C}$ [25]. This is because a stochastic jump, corresponding to the action of a_n on a state in the cat-state subspace, does not cause leakage to the excited eigenstates for large α [25, 70]. We demonstrate the above conclusion in Fig. 3(b), which shows the no-leakage probability

$$P_{\mathcal{C}} = \sum_n {}_n\langle\mathcal{C}_+|\rho(t_g)|\mathcal{C}_+\rangle_n + {}_n\langle\mathcal{C}_-|\rho(t_g)|\mathcal{C}_-\rangle_n \simeq 1, \tag{26}$$

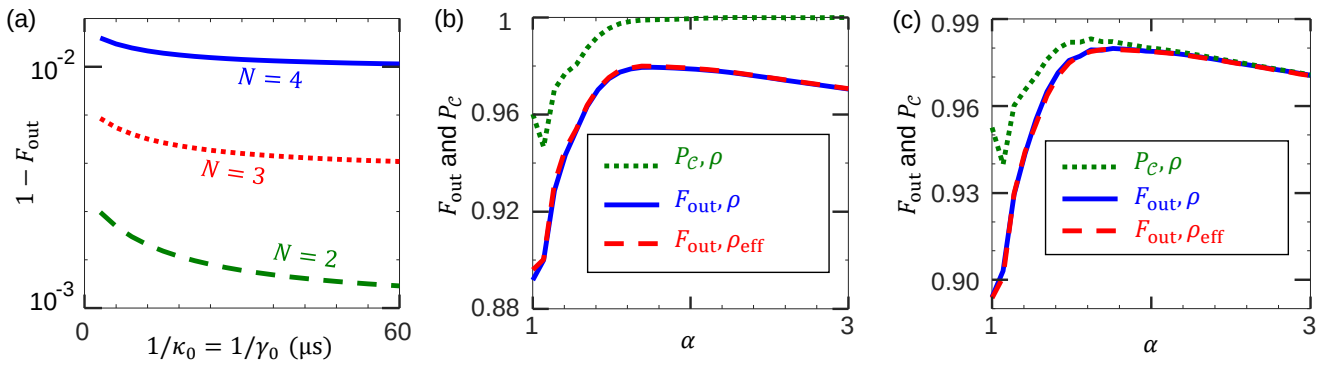

FIG. 3. Numerical results based on the master equations in Eq. (22) and the effective master equation in Eq. (32). (a) Output-state infidelities $(1-F_{\rm out})$ defined in Eq. (24) of the N-qubit gates ($N=2,3,4$) in the presence of decoherence in the cavity mode a_0 when $\alpha=2$. (b, c) Output-state fidelities $F_{\rm out}$ and no-leakage probability $P_{\mathcal{C}}$ of the two-qubit gate versus α when considering only: (b) single-photon loss $\kappa=0.1$ MHz in the KPOs and (c) pure dephasing $\gamma=0.1$ MHz in the KPOs. Note that the blue-solid and green-dotted curves in (b) and (c) are plotted using the Lindblad master equation in Eq. (22). The red-dashed curves in (b) and (c) are plotted for the effective Lindblad master equation in Eq. (32). Other parameters are $J/2\pi=K/2\pi=5$ MHz and $\Delta=4J\alpha$ [i.e., $m=1$ in Eq. (20)], resulting in a gate time $t_g=25$ ns. For clarity, when studying one kind of errors, we assume that the other errors are zero.

for large α. The influence of the single-photon loss in the KPOs is described by the penultimate term in Eq. (25):

$$\begin{aligned}\sum_{n=1}^{N}\kappa_n\mathcal{D}[P_{\rm KPO}a_nP_{\rm KPO}]\rho\approx&\sum_{n=1}^{N}\kappa_n\alpha^2\mathcal{D}\left[\sqrt{\tanh\alpha^2}|\mathcal{C}_+\rangle_n\langle\mathcal{C}_-|+\sqrt{\coth\alpha^2}|\mathcal{C}_-\rangle_n\langle\mathcal{C}_+|\right]\rho\\&+\sum_{n=1}^{N}\kappa_n\mathcal{D}\left[\sqrt{\frac{\mathcal{N}_+}{\mathcal{N}_+^e}}|\mathcal{C}_+\rangle_n\langle\psi_+^{e,1}|+\sqrt{\frac{\mathcal{N}_-}{\mathcal{N}_-^e}}|\mathcal{C}_-\rangle_n\langle\psi_-^{e,1}|\right]\rho\\&+\sum_{n=1}^{N}\kappa_n\alpha^2\mathcal{D}\left[\sqrt{\frac{\mathcal{N}_-^e}{\mathcal{N}_+^e}}|\psi_-^{e,1}\rangle_n\langle\psi_+^{e,1}|+\sqrt{\frac{\mathcal{N}_+^e}{\mathcal{N}_-^e}}|\psi_+^{e,1}\rangle_n\langle\psi_-^{e,1}|\right]\rho.\end{aligned}\tag{27}$$

where we have omitted highly excited eigenstates of the KPOs because they are never excited in the presence of the single-photon loss. According to the terms in the second line in Eq. (27), the single-photon loss can only transfer the excited eigenstates $|\psi_\pm^{e,1}\rangle_n$ to the ground eigenstates $|\mathcal{C}_\pm\rangle_n$. If a KPO is initially in the cat-subspace $\mathcal{C}$, it always remains in this cat-subspace in the presence of the single-photon loss. Therefore, we can neglect the terms in the last two lines in Eq. (27) and obtain (for large α)

$$\mathcal{D}[a_n]\rho\ \simeq\ \frac{\alpha^2}{\sqrt{1-e^{-4\alpha^2}}}\mathcal{D}[\sigma_n^x+ie^{-2\alpha^2}\sigma_n^y]\rho,\tag{28}$$

where $\sigma_n^x=\sigma_n^+ +\sigma_n^-$ and $\sigma_n^y=i(\sigma_n^- -\sigma_n^+)$.

The effective master equation in Eq. (25) becomes

$$\begin{aligned}\dot\rho_{\rm eff}\simeq&-i[P_{\rm KPO}HP_{\rm KPO},\rho_{\rm eff}]+\kappa_0\mathcal{D}[a_0]\rho_{\rm eff}+\gamma_0\mathcal{D}[a_0^\dagger a_0]\rho_{\rm eff}\\&+\frac{\alpha^2}{\sqrt{1-e^{-4\alpha^2}}}\mathcal{D}[\sigma_n^x+ie^{-2\alpha^2}\sigma_n^y]\rho_{\rm eff}+\sum_{n=1}^{N}\gamma_n\mathcal{D}[P_{\rm KPO}a_n^\dagger a_nP_{\rm KPO}]\rho_{\rm eff}.\end{aligned}\tag{29}$$

This means that in the computing subspace the single-photon loss leads primarily to a bit-flip error (σ_n^x), which is accompanied by an exponentially small phase-flip error (σ_n^y). As shown in Fig. 3(b), the full dynamics calculated by Eq. (22) (blue-dotted curve) is in excellent agreement with the effective one using Eq. (28) (red-solid curve) for $\alpha>\sqrt{2}$.

B. Pure dephasing in the Kerr parametric oscillators

The influence of pure dephasing is described by the last term in Eq. (25):

$$\begin{aligned}\sum_{n=1}^{N}\gamma_n\mathcal{D}\left[P_{\rm KPO}a_n^\dagger a_n P_{\rm KPO}\right]\rho=&\sum_{n}^{N}\gamma_n\alpha^4\mathcal{D}\left[\frac{\mathcal{N}_-}{\mathcal{N}_+}|\mathcal{C}_+\rangle_n\langle\mathcal{C}_+|+\frac{\mathcal{N}_+}{\mathcal{N}_-}|\mathcal{C}_-\rangle_n\langle\mathcal{C}_-|\right]\rho\\&+\sum_{n=1}^{N}\gamma_n\alpha^2\mathcal{D}\left[\frac{\mathcal{N}_+}{\sqrt{\mathcal{N}_-\mathcal{N}_+^e}}|\psi_+^{e,1}\rangle_n\langle\mathcal{C}_-|+\frac{\mathcal{N}_-}{\sqrt{\mathcal{N}_+\mathcal{N}_-^e}}|\psi_-^{e,1}\rangle_n\langle\mathcal{C}_+|\right]\rho\\&+\sum_{n=1}^{N}\gamma_n\alpha^4\mathcal{D}\left[\frac{\mathcal{N}_-^e}{\mathcal{N}_+^e}|\psi_+^{e,1}\rangle_n\langle\psi_+^{e,1}|+\frac{\mathcal{N}_+^e}{\mathcal{N}_-^e}|\psi_-^{e,1}\rangle_n\langle\psi_-^{e,1}|\right]\rho.\end{aligned}\tag{30}$$

As in the above analysis, we have ignored the highly excited eigenstates of the KPOs because they are mostly unexcited in the evolution. According to the terms in the second line in Eq. (30), pure dephasing can cause transitions from the cat states to the first-excited states with a rate $\gamma_n\alpha^2$. This cause infidelities to the system. For a large α, we have $\mathcal{N}_\pm\simeq\mathcal{N}_\pm^e\simeq 2$, and Eq. (30) becomes (choosing $\gamma_n=\gamma$)

$$\sum_{n=1}^{N}\gamma_n\mathcal{D}[a_n^\dagger a_n]\rho\simeq\gamma\sum_{n=1}^{N}\alpha^4\mathcal{D}[\mathbb{1}_n]\rho+\alpha^2\mathcal{D}\left[\sum_{k=\pm}|\psi_k^e\rangle_n\langle\mathcal{C}_k|+\text{h.c.}\right]\rho.\tag{31}$$

That is, in the computational subspace for large α, pure dephasing cannot cause significant infidelities. We can further simplify the master equation in Eq. (29) to be

$$\begin{aligned}\dot\rho_{\rm eff}\simeq&-i[P_{\rm KPO}HP_{\rm KPO},\rho_{\rm eff}]+\kappa_0\mathcal{D}[a_0]\rho_{\rm eff}+\gamma_0\mathcal{D}[a_0^\dagger a_0]\rho_{\rm eff}\\&+\frac{\alpha^2}{\sqrt{1-e^{-4\alpha^2}}}\mathcal{D}[\sigma_n^x+ie^{-2\alpha^2}\sigma_n^y]\rho_{\rm eff}+\gamma\sum_{n=1}^{N}\alpha^4\mathcal{D}[\mathbb{1}_n]\rho_{\rm eff}.\end{aligned}\tag{32}$$

Therefore, when considering the single-photon loss and pure dephasing, the only remaining error in the computational subspace is the bit flip characterized by the operator σ_n^x, which commutes with the evolution operator $U_{\rm MS}(t)$. Therefore, an erroneous gate operation is equivalent to an error-free gate followed by an error σ_n^x. Therefore, our cat-code gates preserve the error bias.

To be specific, we can assume that the dominant error σ_n^x occurs in one of the cat-state qubits at time $\tau_{\rm err}$ ($0<\tau_{\rm err}<t_g$). Then, the evolution should be modified as

$$U_{\rm MS}^{\rm err}(t_g)=U_{\rm MS}(t_g-\tau_{\rm err})\sigma_x^nU_{\rm MS}(\tau_{\rm err}).\tag{33}$$

As shown in our manuscript, the evolution operator $U_{\rm MS}(t)$ reads

$$U_{\rm MS}(t)=\exp\left[-i\chi(t)a_0^\dagger S_x+\text{h.c.}\right]\exp\left[-i\beta(t)S_x^2\right],\tag{34}$$

where $S_x=\frac{1}{2}\sum_n\sigma_n^x$ commutes with the dominant error σ_n^x. Therefore, we obtain

$$U_{\rm MS}^{\rm err}(t_g)=\sigma_x^nU_{\rm MS}(t_g),\tag{35}$$

which indicates that our cat-code MS gate preserves the error bias.

However, pure dephasing in the KPOs causes transitions to the excited eigenstates $|\psi_\pm^{e,1}\rangle_n$ [the last term in Eq. (31)] [25]. Such transitions cause an infidelity $(1-F_{\rm out})$ that is equivalent to the leakage probability $(1-P_{\mathcal{C}})$. This is demonstrated in Fig. 3(c) that $P_{\mathcal{C}}\simeq F_{\rm out}$ in the presence of only pure dephasing in the KPOs. Hence, in experiments to realize our protocol, it would be better to choose systems with small dephasing rates.

V. PARAMETER IMPERFECTIONS

In addition to decoherence, parameter imperfections may also cause infidelities. In the presence of parameter imperfections, a parameter $*$ should be corrected as $*'=*\pm\delta*$, where $\delta*$ denotes the noise. For clarity, the noise-disturbed gate fidelity is expressed as $\bar F_N(\delta*)$. We consider two kinds of noise: stochastic and systematic. For the stochastic noise, the noise rate $(\delta*)/*$ is a time-dependent random number; and can be expressed as a random number $(\delta*)/*=\text{rand}(\epsilon_s)$ in the interval $(-\epsilon_s,\epsilon_s)$. For instance, we consider stochastic noise in the parameters J and Δ. The actual values of J and Δ should be corrected as

$$\begin{aligned}J(t_\eta)=&J\left[1\pm\text{rand}(\epsilon_s)\right],\\\Delta(t_\eta)=&\Delta\left[1\pm\text{rand}(\epsilon_s)\right].\end{aligned}\tag{36}$$

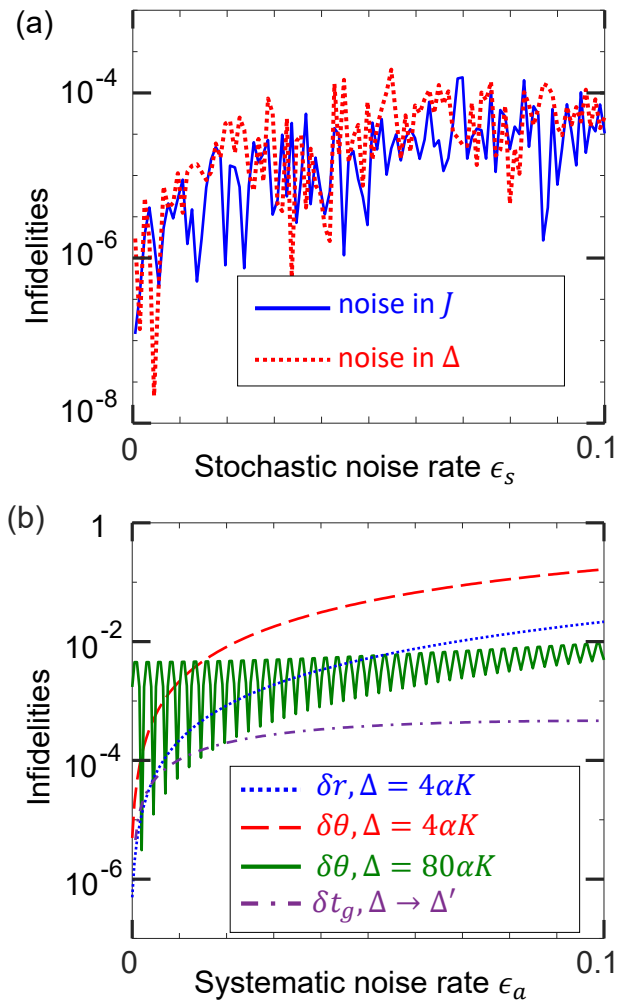

FIG. 4. Noise-induced infidelities of the two-qubit gate when $\alpha = 2$ calculated for the total Hamiltonian H in the presence of parameter imperfections. (a) Infidelities $|\bar{F}_2(\epsilon_s) - \bar{F}_2(0)|$ versus stochastic noise rate ϵ_s. (b) Infidelities $|\bar{F}_2(\epsilon_a) - \bar{F}_2(0)|$ versus systematic noise rate ϵ_a. Here, the gate fidelity $\bar{F}_2$ is defined in Eq. (18). To aim at the influence of parameter imperfections, we assume the decay rates $\gamma = \kappa = 0$. For (a) we choose $J/2\pi = K/2\pi = 5$ MHz and $\Delta = 4J\alpha$ ($m = 1$), resulting in a gate time $t_g = 25$ ns. For (b), when discussing a kind of noise, e.g., δr, we ignore the other noises. The purple-dashed-dotted curve is calculated by changing the detuning $\Delta/2\pi = \sqrt{0.95} \times 40$ MHz to $\Delta'/2\pi = \sqrt{0.05} \times 40$ MHz at the time $\tau = 0.95 t_g$.

Here, t_η means that, at the time $0 < t_\eta < t_g$, the noise arises the ηth time. Assuming that the noise randomly arises a total of $1,000$ times, the noise-induced infidelities $\left|\bar{F}_N(\epsilon_s) - \bar{F}(0)\right|$ are very small, as shown in Fig. 4(a). A noise rate $\epsilon_s = 0.1$ only causes an infidelity $\sim 10^{-4}$, indicating that the gates are mostly insensitive to stochastic noise. The oscillations in the gate infidelities demonstrate that the stochastic noise randomly affects the system.

For the systematic noise, the noise rate $(\delta*)/* = \epsilon_a$ becomes a small constant. According to the evolution operator $U_{\rm MS}(t)$, parameter imperfections may induce deviations in the radius r and the rotation angle θ that cause infidelities. For simplicity, we can analyze the influence of imperfections in r (caused by the imperfections in J, α, or $1/\Delta$) and θ (caused by the imperfections in Δ or t_g). As shown in Fig. 4(b), the imperfections in θ (red-dashed curve) have a greater influence than those of r (blue-dotted curve) when fixing the detuning Δ. This is because $\delta\theta$ can cause excitations in the cavity mode a_0 [i.e., $\chi(t_g) \neq 0$ in $U_{\rm MS}(t_g)$], leading to infidelities. These excitations can be suppressed by increasing the detuning Δ [see the green-solid curve in Fig. 4(b)], because $\chi(t)$ is inversely proportional to Δ.

However, a larger detuning means a longer gate time, which increases the influence of decoherence. Note that the imperfections in θ are mainly caused by the imperfections in the gate time t_g, which affects the system in the time interval $t_g\,(1-\epsilon_a,\ 1+\epsilon_a)$. We can increase Δ only in this time interval to minimize the influence on the gate time. For this goal, we choose

$$\Delta = \frac{4\sqrt{m}J\alpha}{\sqrt{1-\epsilon_a}}, \quad \text{and} \quad \tau = t_g(1-\epsilon_a) = \frac{2\pi m}{\Delta}, \tag{37}$$

to satisfy $\chi(\tau) = 0$. Then, the detuning is increased to $\Delta' = 4\sqrt{m'}J\alpha/\sqrt{\epsilon_a}$, where m' denotes the number of evolution cycles in phase space in the time interval $t_g\,(1-\epsilon_a,\ 1)$. These parameters ensure that the total geometric phase is still $\beta(t_g) = -\pi/2$. The gate time becomes

$$t_g = \frac{\pi}{2J\alpha}\left[\sqrt{m(1-\epsilon_a)} + \sqrt{m'\epsilon_a}\right] \approx \frac{\sqrt{m}\pi}{2J\alpha},$$

for $m \geq m'$ and $\epsilon_a \ll 1$. Therefore, the gate time is mostly unchanged, while we can achieve the gate robustness against its parameter imperfections [see the purple-dot-dashed curve in Fig. 4(b)].

VI. DISCUSSION

Using the above optimized method, when decoherence and parameter imperfections are considered, the fidelities of the output states for $N = 2, 3, 4$ are shown in Fig. 5. The rates of the systematic noise are chosen as:

$$\delta J/J = \delta\Delta/\Delta = \delta\Delta'/\Delta' = \delta t_g/t_g = -5\%. \tag{38}$$

We ignore the stochastic noise because it, practically, does not affect the system dynamics. Superconducting circuits [5, 74, 90–96] can be a possible implementation of our protocol (see details in the Appendix C). For instance, one can use the Josephson parametric amplifier [4, 5, 81, 94, 97–105] to realize the Hamiltonian $H_n^{\rm Kerr}$. Another especially promising setup to realize our protocol could be a single junction or transmon embedded

TABLE I. Fidelities of quantum gates based on bosonic codes. Coherence properties: Energy relaxation time ($T_1 = 1/\kappa_j$) and dephasing time ($T_2^* = 1/\gamma_j$).

Year	Code	Gate Type	T_1 (μs)	T_2^* (μs)	Fidelity (%)
2017 [29]	Cat	Single-qubit gates	~ 170	~ 43	98.5
2018 [32]	Binomial	CNOT	~ 2000	~ 500	89.0
2018 [31]	Binomial	Teleported CNOT	~ 1000	~ 300	79.0
2019 [88]	Binomial	Single-qubit gates	~ 140	~ 250	97.0
2019 [89]	Fock	eSWAP	$\gtrsim 200$	$\gtrsim 300$	85.0
2020 [34]	Binomial & Cat	Geometric cPhase	$\gtrsim 500$	$\gtrsim 300$	89.4
Our protocol	Cat	Two-qubit MS gate	~ 200	~ 200	~ 98
		Three-qubit MS gate			~ 97
		Four-qubit MS gate			~ 90

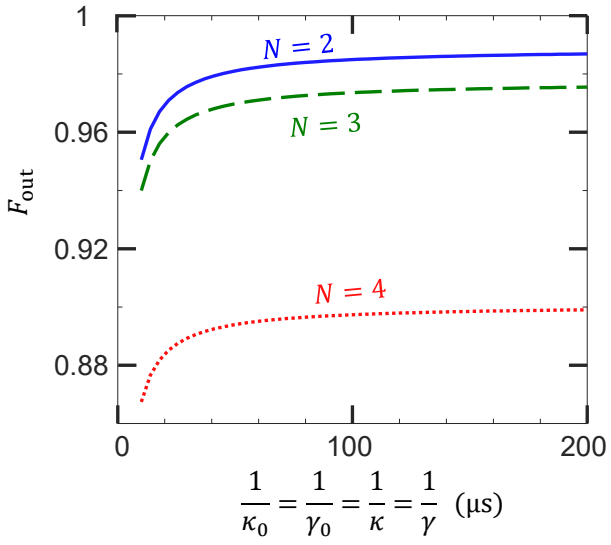

FIG. 5. Output-state fidelities $F_{\rm out}$ of the N-qubit gates in the presence of decoherence and parameter imperfections. Here, $F_{\rm out}$ is calculated using the Lindblad master equation Eq. (22) for the total Hamiltonian H in the presence of parameter imperfections. Parameters are $J/2\pi = K/2\pi = 5$ MHz and $\alpha = 2$. We choose systematic noise rates $\delta J/J = \delta\Delta/\Delta = \delta\Delta'/\Delta' = \delta t_g/t_g = -\epsilon_a = -5\%$. We change the detuning $\Delta/2\pi = \sqrt{0.95}\times 40$ MHz to $\Delta'/2\pi = \sqrt{0.05}\times 40$ MHz at the time $\tau = 0.95t_g$, to suppress the error induced by parameter imperfections in the gate time.

in a 3D oscillator [15, 16]. The Kerr nonlinearity and the two-photon drive can be respectively realized by the Josephson junction (transmon) nonlinearity and four-wave mixing [25, 106–109]. The change of detuning can be generally realized by changing the frequency ω_c (see the Appendix D for more details). Such a change should be as fast as possible to avoid introducing an additional phase shift.

Note that the cat-state qubits discussed in our manuscript belong to a larger family of bosonic qubits. Bosonic-code quantum gates have been realized using superconducting circuit quantum electrodynamics (circuit QED) architecture and three-dimensional (3D) cavities, especially 3D coaxial cavities. The experimental platforms that have already realized different bosonic qubits could implement bosonic cat-state qubits [15, 16]. For instance, Ref. [34] reported an experimental realization of both binomial and cat-state qubits using the same experimental platform. For clarity, we show the fidelities and the corresponding coherence properties of some one- and two-qubit gates in Table I, which have been realized in current experiments. As shown, current experiments are still challenging to achieve high-fidelity bosonic gates, which may lower the code-capacity threshold for error correction.

Geometric quantum gates with cat-state qubits were recently experimentally realized in 2020 [34]. With coherence times $T_1 = 1/\kappa_j \sim 500$ μs and $T_2^* = 1/\gamma_j \sim 300$ μs, that experiment [34] only realized two-qubit gates with fidelities $\sim 90\%$. In contrast to this, our protocol can easily generate a two-qubit gate with fidelities $\gtrsim 90\%$ even when using much shorter coherence times [blue-solid curve in Fig. 5]. For the implementation shown in Appendix C, the experimental coherence times for the Kerr parametric oscillator can reach $T_1 \sim T_2^* \sim 15 \gtrsim \mu$s [104], which enable our protocol to generate two-, three-, and four-qubit gates with fidelities $\sim 97.5\%$, $\sim 94\%$, and $\sim 86\%$, respectively.

VII. CONCLUSIONS

We have investigated the possibility of using photonic cat-state qubits for implementing multiqubit geometric gates, which can generate maximally multi-mode entangled cat states with high fidelities. Our theoretical protocol is robust against stochastic noise along the evolution path because of the character of the geometric evolution. By increasing the detuning at a suitable time, the protocol can tolerate imperfections in the gate time. For large α, the phase-flip error can be exponentially suppressed, leaving only the bit-flip error. The pure

dephasing of the cavity modes may lead to the photon leakage out of the computing subspace, but does not cause qubit-dephasing problems for the system. This dominant error commutes with the evolution operator, which makes our MS gates preserving the error bias. Therefore, error-correction layers can focus on only the bit-flip error using less physical resources. In summary, our results offer a realistic and hardware-efficient method for multiqubit fault-tolerant quantum computation.

Appendix A: Arbitrary single-qubit rotations of cat-state qubits

Accompanied by a variety of single-qubit rotations, the Mølmer-Sørensen gate can be adapted to many quantum algorithms, such as Grover's quantum search algorithm [3, 55, 56]. To realize such single-qubit rotations, one needs to add a single-photon drive to each KPO [74]. The Hamiltonian for each KPO becomes

$$\begin{aligned}\tilde{H}_n^{\rm Kerr} =&\Omega_p\left(a_n^{\dagger 2}+a_n^2\right)-Ka_n^{\dagger 2}a_n^2\\&+\Delta_q a_n^\dagger a_n+(\xi_p a_n+\xi_p^* a_n^\dagger),\end{aligned}\tag{A1}$$

where ξ_p is the complex driving amplitude. Note that the parameters discussed in this section are independent of those in the main text and Sec. S1. When

$$\Delta_q,|\xi_p|\ll E_{\rm gap},\tag{A2}$$

the evolution is restricted in the cat-state subspace $\mathcal{C}$. The effective Hamiltonian in the cat-subspace reads ($\alpha=\alpha^*=\sqrt{\Omega_p/K}$):

$$\begin{aligned}\tilde{H}_{n,\rm eff}^{\rm Kerr} =&\frac{1}{2}\Delta_q\alpha^2\left(\coth\alpha^2-\tanh\alpha^2\right)\sigma_n^z\\&+\left[\left(\xi\alpha\sqrt{\tanh\alpha^2}+\xi^*\alpha\sqrt{\coth\alpha^2}\right)\sigma_n^-+\text{h.c.}\right]\\=&\frac{\tilde{\Delta}_q}{2}\sigma_n^z+\left[\Omega_1\exp\left(-i\varphi\right)\sigma_n^-+\text{h.c.}\right],\end{aligned}\tag{A3}$$

where $\sigma_n^z=|\mathcal{C}_-\rangle_n\langle\mathcal{C}_-|-|\mathcal{C}_+\rangle_n\langle\mathcal{C}_+|$.

Obviously, the effective Hamiltonian $\tilde{H}_{n,\rm eff}^{\rm Kerr}$ contains all the Pauli matrixes for a two-level system. Thus, it can realize arbitrary single-qubit rotations. The evolution operator in matrix form becomes

$$U_1=\exp\left(-i\tilde{H}_{n,\rm eff}t\right)=\begin{pmatrix}\cos(\Xi t)-i\sin(\Xi t)\cos\theta & -i\exp\left(-i\varphi\right)\sin(\Xi t)\sin\theta\\ -i\exp\left(i\varphi\right)\sin(\Xi t)\sin\theta & \cos(\Xi t)+i\sin(\Xi t)\cos\theta\end{pmatrix},$$

which denotes an arbitrary rotation on the Bloch sphere [see Fig. 6(a)]. Here,

$$\begin{aligned}\Xi&=\sqrt{\tilde{\Delta}_q^2/4+\Omega_1^2},\\\theta&=\arctan(2\Omega_1/\tilde{\Delta}_q).\end{aligned}\tag{A4}$$

For instance, when $\Xi t=\pi/2$, $\theta=\pi/4$, and $\varphi=0$, U_1 denotes the Hadamard gate up to a global phase $\pi/2$ [see the blue-dashed curve in Fig. 6(b)]. When $\Xi t=\pi/2$, $\theta=\pi/2$, and $\varphi=0$, U_1 becomes the NOT gate up to a global phase $\pi/2$ [see the red-solid curve in Fig. 6(b)]. We can see in Fig. 6(b) that the gate time of the Hadamard gate is much longer than that of the NOT gate. This is understood because the effective detuning $\tilde{\Delta}_q$ exponentially decreases when α increases. Thus, it takes a long time to obtain a phase rotation about the z axis.

As an alternative to obtaining a large effective detuning $\tilde{\Delta}_q$, one can employ an interaction Hamiltonian

$$\begin{aligned}H_{\rm add}(t)=&\xi_J\cos\left[\varphi_a(a_ne^{-i\omega_c t}+a_n^\dagger e^{i\omega_c t})\right]\\=&\frac{\xi_J}{2}\left[D_n(\beta_t)+D_n(-\beta_t)\right],\end{aligned}\tag{A5}$$

which can be realized by strongly coupling a high impedance cavity mode to a Josephson junction [75–77]. Here, ξ_J is the effective Josephson energy and $\varphi_a=\sqrt{Z_a/2R_Q}$, with Z_a and R_Q being the impedance of the cavity mode seen by the junction and the superconducting resistance quantum, respectively. The displacement parameter is

$$\beta_t=i\varphi_a\exp\left(i\omega_c t\right).\tag{A6}$$

When $\omega_c,E_{\rm gap}\gg\xi_J$ and $\varphi_a\simeq 2\alpha$, the effective Hamiltonian under the rotating wave approximation in the cat-state subspace becomes [77]

$$\tilde{H}_{\rm add}=\frac{\tilde{\Delta}_q}{2}\sigma_n^z,\tag{A7}$$

where $\tilde{\Delta}_q\simeq\xi_J/\alpha\sqrt{2\pi}$. Substituting Eq. (A7) into Eq. (A3) and assuming $\Delta_q=0$, the evolution operator still takes the form of Eq. (A4). Figure 6(c) shows the average infidelities of the Hadamard gate when the additional Hamiltonian $H_{\rm add}(t)$ is added. Comparing to the result in Fig. 6(b), the additional Hamiltonian $H_{\rm add}(t)$ obviously increases the effective detuning, so that

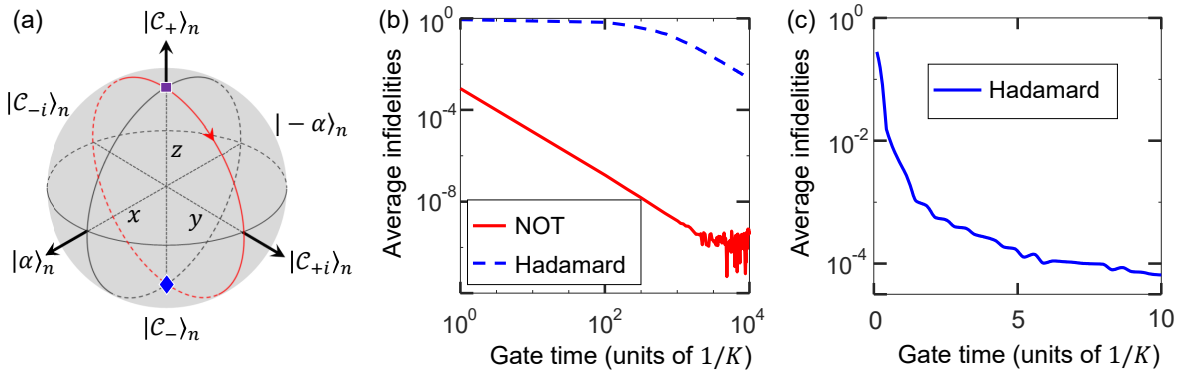

FIG. 6. (a) Bloch sphere of the cat qubit in the limit of large α (i.e., $\alpha = 2$). The red circle with a red arrow denotes the evolution path for the NOT gate. For instance, when the input state is $|\mathcal{C}_+\rangle_n$ (purple square), the NOT gate transforms this input state into $|\mathcal{C}_-\rangle_n$ (blue diamond). The states on all y axis are $|\mathcal{C}_{\pm i}\rangle_n \simeq (|\alpha\rangle_n \pm i|-\alpha\rangle_n)/\sqrt{2}$. (b) Average infidelities of the Hadamard and NOT gates versus the gate time calculated via the Hamiltonian in Eq. (A1). (c) Average infidelities of the Hadamard gate when the additional Hamiltonian in Eq. (A5) is added, i.e., when the total Hamiltonian is $H_{\rm tot}(t) = \tilde{H}_n^{\rm Kerr} + H_{\rm add}(t)$. We assume that the frequency of each KPO is $\omega_c = 800K$ and the coherent-state amplitude is $\alpha = 2$. Other parameters are given below Eq. (A4).

the gate time is shortened. For instance, a gate time $\sim 5/K \approx 8$ ns (for $K/2\pi \sim 10$ MHz) is enough to achieve a Hadamard gate with a fidelity $\gtrsim 99.99\%$.

Appendix B: Preparing Schrödinger cat states

To generate the quantum cat states in the KPOs, we first decouple the KPOs from the common cavity a_0 by tuning $J = 0$ or $\Delta = \infty$. Then, we change the Hamiltonian for each KPO to be time-dependent [we assume $t \in [-t_0, 0]$ and $\Omega_p(t) = \Omega_p^*(t) \geq 0$ for simplicity]:

$$H_n^{\rm Kerr}(t) = \Omega_p(t)\left(a_n^{\dagger 2} + a_n^2\right) - K a_n^{\dagger 2} a_n^2 + \Delta_q(t) a_n^\dagger a_n, \tag{B1}$$

where $\Delta_q(t) = \omega_c - \omega_p/2$ is a time-dependent detuning and t_0 denotes the total evolution time required for the generation of cat states. To study the dynamics of the time-dependent Hamiltonian $H_n^{\rm Kerr}(t)$, we introduce the displacement operators $D_n(\pm\alpha_t) = \exp\left(\pm\alpha_t a_n^\dagger \mp \alpha_t a_n\right)$ to transform $H_n^{\rm Kerr}(t)$ as

$$\begin{aligned} H_n'(t) =& D_n(\pm\alpha_t) H_n^{\rm Kerr}(t) D_n(\mp\alpha_t) - i D_n(\pm\alpha_t)\dot{D}_n(\mp\alpha_t) \\ =& \left[\Delta_q(t) - 4K\alpha_t^2\right] a_n^\dagger a_n \mp 2K\alpha_t\left(a_n^{\dagger 2} a_n + a_n^\dagger a_n^2\right) \\ & - K a_n^{\dagger 2} a_n^2 \mp \left[\alpha_t \Delta_q(t) + i\dot{\alpha}_t\right] a_n^\dagger \\ & \mp \left[\alpha_t \Delta_q(t) - i\dot{\alpha}_t\right] a_n, \end{aligned} \tag{B2}$$

where $\alpha_t = \sqrt{\Omega_p(t)/K} \geq 0$ is the time-dependent amplitude of a coherent state $|\alpha_t\rangle$.

Obviously, when

$$\left[\Delta_q(t) - 4K\alpha_t^2\right] \gg 2K\alpha_t,$$

$$\left[\Delta_q(t) - 4K\alpha_t^2\right] \gg \sqrt{\left[\alpha_t \Delta_q(t)\right]^2 + \dot{\alpha}_t^2}, \tag{B3}$$

the Hamiltonian $H_n'(t)$ cannot change the photon number of the system in the displacement frame. In this case, when α_t satisfies the boundaries

$$\alpha_t|_{t=-t_0} = 0, \quad \text{and} \quad \alpha_t|_{t=0} = \alpha. \tag{B4}$$

Assuming that the system in the displaced frame is in the displaced vacuum state $|0\rangle_n$ at the time $-t_0$, the evolution in the lab frame can be described by

$$|\psi(t)\rangle_n = D_n(\pm\alpha_t)|0\rangle_n, \tag{B5}$$

or can be equivalently described by

$$|\psi(t)\rangle_n = \mathcal{N}_\pm(\alpha_t)\left[D_n(\alpha_t) \pm D_n(-\alpha_t)\right]|0\rangle_n, \tag{B6}$$

where $\mathcal{N}_\pm(\alpha_t) = 1/\sqrt{2\left[1 \pm \exp(-2\alpha_t^2)\right]}$.

To satisfy the condition in Eq. (B3), for $t \leq 0$, we assume $\alpha_t = \alpha$ and $\Delta_q(t) = 0$, while for $(t_0 \leq t < 0)$ we assume

$$\begin{aligned} \alpha_t &= \frac{\alpha}{t_0}(t + t_0), \\ \Delta_q(t) &= -K \sin\left[\frac{\pi}{t_0}(t + t_0)\right]. \end{aligned} \tag{B7}$$

Then, at $t = 0$, the desired cat states $|\mathcal{C}_\pm\rangle_n = |\psi(0)\rangle_n$ can be generated. The driving amplitude $\Omega_p(t)$ and the detuning $\Delta_q(t)$ using the parameters in Eq. (B7) are shown in Fig. 7(a). In the absence of decoherence, the fidelities

$$F_\pm = {}_n\langle\mathcal{C}_\pm|\rho(0)|\mathcal{C}_\pm\rangle_n, \tag{B8}$$

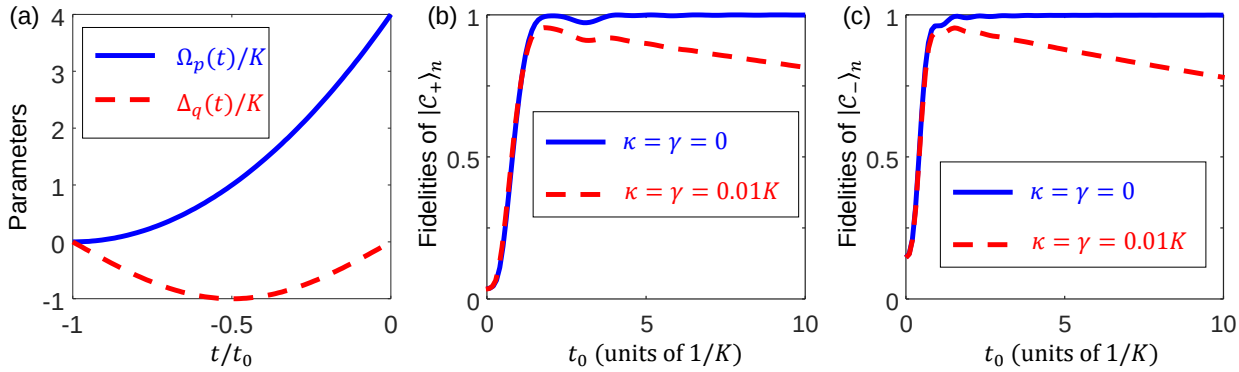

FIG. 7. (a) Parameters used for the generation of the cat states $|\mathcal{C}_\pm\rangle_n$. Fidelities of (b) the even cat state $|\mathcal{C}_+\rangle_n$ and (c) the odd cat state $|\mathcal{C}_-\rangle_n$ versus the total evolution time t_0 calculated for the Hamiltonian in Eq. (B1). The initial states for (b) is $|\psi(-t_0)\rangle_n=|0\rangle_n$ and (c) is $|\psi(-t_0)\rangle_n=|1\rangle_n$. Other parameters are given in Eq. (B7).

of the prepared cat states are shown in Fig. 7(b) and Fig 7(c). As a result, an evolution time $t_0\gtrsim 1.7/K\approx$ 3 ns (when $K/2\pi=10$ MHz) is enough to generate the cat states $|\mathcal{C}_\pm\rangle_n$ with fidelities $\gtrsim 99\%$. In the presence of decoherence, for the nth KPO, the dynamics is described by the Lindblad master equation

$$\dot{\rho}_n=-i[H_n^{\rm Kerr}(t),\rho_n]+\kappa\mathcal{D}[a_n]\rho_n+\gamma\mathcal{D}[a_n^\dagger a_n]\rho_n, \quad \text{(B9)}$$

where

$$\mathcal{D}[o]\rho_n=o\rho_n o^\dagger-\frac{1}{2}\left(o^\dagger o\rho_n+\rho_n o^\dagger o\right) \quad \text{(B10)}$$

is the Lindblad superoperator, κ is the single-photon loss rate, and γ is the pure dephasing rate. In Fig. 7(b) and Fig. 7(c), we can see that the fidelities of the cat states can be higher than 95% when the decay rates are $\kappa=\gamma=0.01K$.

Appendix C: A possible implementation using superconducting quantum interference devices

A possible implementation for our protocol can be based on superconducting quantum interference devices (SQUIDs). For instance, the KPOs can be realized using an array of Josephson junctions. Such quantum parametric oscillators have been experimentally realized, in e.g, Ref. [81]. We can then embed these parametric oscillators (with a relatively long distance to each other) in a transmission-line resonator [see Fig. 8(a)]. The transmission-line resonator can be modeled by an LC oscillator [see Fig. 8(b)] and it is used as the cavity mode a_0 in our protocol. The direct coupling between two adjacent KPOs can be neglected because of the long distance between them.

Following the standard quantization procedure for circuits, the Hamiltonian for the circuit in Fig. 8(b) is

$$\begin{aligned}H_n=&\frac{\hat{\phi}_r^2}{2L_r}+\frac{(C_B+C_g)\hat{Q}_r^2}{2C_*}\\&+\frac{(C_g+C_{\rm in}+C_r)\hat{Q}_J^2}{2C_*}-N_0E_J[\Phi(t)]\cos\frac{\hat{\phi}}{N_0}\\&+\frac{C_g\hat{Q}_r\hat{Q}_J}{C_*},\end{aligned} \quad \text{(C1)}$$

where

$$C_*=C_BC_g+C_BC_{\rm in}+C_gC_{\rm in}+C_BC_r+C_gC_r. \quad \text{(C2)}$$

The subscript n denotes that this is the Hamiltonian describing the coupling between the nth KPO and the cavity mode a_0. The first line in H_n describes the local oscillator of the resonator a_0; the second line is the Hamiltonian for the KPO; and the third line describes the coupling. Here, $\hat{Q}_r$ and $\hat{Q}_J$ are charges for the LC resonator and the array of Josephson junctions, respectively; $\hat{\phi}_r$ and $\Phi(t)$ are the branch and external-magnetic fluxes for modulating the energies of the quantum LC circuit and the KPO, respectively; N_0 is the number of SQUIDs in the array; and E_J is the Josephson energy of a single SQUID.

In the realistic limit of large resonator capacitance $C_r\gg(C_B+C_g)$, we can simplify the Hamiltonian H_n as

$$\begin{aligned}H_n=&\omega_0a_0^\dagger a_0+4E_C\hat{n}^2-N_0E_J[\Phi(t)]\cos\frac{\hat{\phi}}{N_0}\\&+\frac{2C_geV_{\rm rms}^0}{C_g+C_B}(a_0+a_0^\dagger)\hat{n}.\end{aligned} \quad \text{(C3)}$$

Here, $\hat{n}$ and $\hat{\phi}$ are the number of Cooper pairs and the overall phase across the junction array, respectively; E_C is the KPO charging energy, and $\omega_0=1/\sqrt{L_rC_r}$ denotes the frequency of the cavity mode a_0. Moreover, The root-mean-square voltage of the local oscillator is denoted by $V_{\rm rms}^0=\sqrt{\omega_0/2C_r}$.

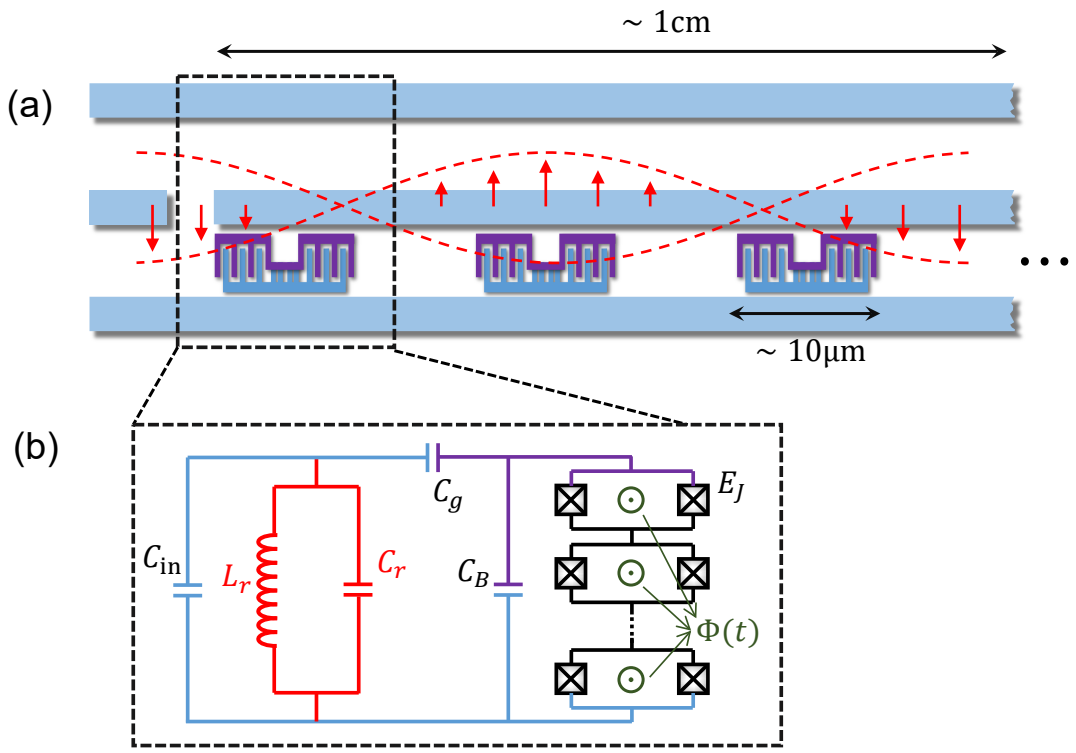

FIG. 8. (a) Simplified schematic of the transmon device design, which consists of several KPOs, shunted by a short section of a twin-lead transmission line. This short section of line can be well approximated as a lumped-element capacitor. (b) Effective circuit diagram of a KPO coupled to an LC oscillator. The KPO is realized using an array of Josephson junctions, in which the Josephson energy E_J is tunable by controlling the external magnetic flux $\Phi(t)$. The array of Josephson junctions with capacitance and Josephson energy C_J and E_J are shunted by an additional large capacitance C_B, matched by a comparably large gate capacitance C_g. Following the standard quantization procedure for circuits [90, 91], we have absorbed the junction capacitance C_J into the parallel capacitance C_B for simplicity.

We assume that the Josephson energy E_J is modified as (with a frequency ω_p)

$$E_J[\Phi(t)] = E_J + \delta E_J \cos(\omega_p t). \tag{C4}$$

After applying the Taylor expansion of $\cos\left(\hat{\phi}/N_0\right)$ to fourth order, we obtain

$$\begin{aligned} H_n \approx\ & \omega_0 a_0^\dagger a_0 + 4E_C\hat{n}^2 - N_0 E_J(1 - \hat{X} + \hat{X}^2/6) \\ & - N_0\delta E_J(1-\hat{X})\cos(\omega_p t) \\ & + \frac{2C_g e V^0_{\text{rms}}}{C_g + C_B}(a_0 + a_0^\dagger)\hat{n}, \end{aligned} \tag{C5}$$

where $\hat{X} = (\hat{\phi}/N_0)^2/2$. We assume that the system is not highly excited, i.e., the highest level is much smaller than the dimension of the Hilbert space. Then, following the standard quantization procedure for circuits [90, 91], we can define ($\hbar = 1$)

$$\begin{aligned} \hat{n} =& -in_0(a_n - a_n^\dagger), \\ \hat{\phi} =& \phi_0(a_n + a_n^\dagger), \end{aligned} \tag{C6}$$

where $n_0 = \sqrt[4]{E_J/(32N_0E_C)}$ and $\phi_0 = 2\sqrt{2}/n_0$ are the zero-point fluctuations. The quadratic time-independent part of the Hamiltonian H_n can be diagonalized and the Hamiltonian H_n becomes

$$\begin{aligned} H_n =\ & \omega_0 a_0^\dagger a_0 + \omega_c a_n^\dagger a_n - \frac{E_C}{12N_0^2}\left(a_n + a_n^\dagger\right)^4 \\ & + \frac{\delta E_J \omega_c}{4E_J}\left(a_n + a_n^\dagger\right)^2\cos(\omega_p t) \\ & + \frac{2C_g e V^0_{\text{rms}} n_0}{C_g + C_B}(a_0 + a_0^\dagger)(ia_n^\dagger - ia_n) \end{aligned} \tag{C7}$$

where $\omega_c = \sqrt{8E_C E_J/N_0}$. Here, we have dropped the constant terms for simplicity.

We assume that the two-photon drive is resonant with the cavity mode, i.e., $2\omega_p = \omega_c$. When the conditions

$$\begin{aligned} \omega_p \gg & \frac{E_C}{12N_0^2}, \\ \omega_p \gg & \frac{\delta E_J \omega_c}{4E_J}, \\ \omega_p \gg & \frac{2C_g e V^0_{\text{rms}} n_0}{C_g + C_B}, \end{aligned} \tag{C8}$$

are satisfied, the counter-rotating terms in Eq. (C7) can be neglected under the rotating-wave approximation.

The effective Hamiltonian of the system in the interaction frame becomes

$$H_n = -Ka_n^{\dagger 2}a_n^2 + \Omega_p(a_n^{\dagger 2} + a_n^2) + \left[Ja_n a_0^\dagger \exp(i\Delta t) + \text{h.c.}\right], \tag{C9}$$

where $K = 2E_C/N_0^2$, $\Omega_p = \delta E_J \omega_c/8E_J$, $J = -i2C_g eV_{\text{rms}}^0 n_0/(C_g + C_B)$, and $\Delta = \omega_0 - \omega_c$. We have assumed above that the direct coupling between two adjacent KPOs can be neglected because of the long distance between them. The total Hamiltonian for the device in Fig. 8(a) is

$$H = \sum_{n=1}^{N} H_n = \sum_{n=1}^{N} -Ka_n^{\dagger 2}a_n^2 + \Omega_p(a_n^{\dagger 2} + a_n^2) + \left[Ja_n a_0^\dagger \exp(i\Delta t) + \text{h.c.}\right], \tag{C10}$$

which is the Hamiltonian used for our protocol.

Appendix D: Changing the detuning Δ

The change of the detuning Δ can be generally realized using two approaches by: (a) changing the frequency ω_c of the KPOs and (b) inducing a Stark shift for the cavity mode a_0. Both approaches can be realized by changing the external magnetic flux for transmon qubits. A frequency-tunable cavity a_0 is also a solution for this goal, but it is relatively difficult to experimentally change the inductance L_r or the capacitance C_r.

For the (a) approach, according to Eq. (C7), one can chance the frequency $\omega_c = \sqrt{8E_C E_J/N_0}$ for each KPO by changing the flux-dependent Josephson energy $E_J \to E_J'$. Note that, when E_J is changed, one needs to adjust the modification $\delta E_J \to \delta E_J'$ to satisfy $\delta E_J'/E_J' = \delta E_J/E_J$, so that the two-photon driving amplitude Ω_p remains unchanged.

For the (b) approach, we can choose one of the KPOs to be an auxiliary transmon qubit by reducing the number N_0 of Cooper pairs, e.g., we can assume $N_0 = 1$ for the auxiliary transmon qubit. This auxiliary transmon qubit and the cavity mode a_0 is designed to be far off-resonant, i.e., their detuning Δ_a is much larger than their coupling strength J_a. Then, we arrive at the dispersive Hamiltonian

$$H_{0,a} = \Delta_s |e\rangle_a\langle e| a_0^\dagger a_0, \tag{D1}$$

where $\Delta_s = J_a^2/\Delta_a$ is the Stark shift and $|e\rangle_a$ is the excited state of the auxiliary transmon qubit. In this case, when we restrict the auxiliary transmon qubit to be in its ground state, Eq. (D1) corresponds to a modification for the frequency of the cavity mode a_0. The total Hamiltonian becomes

$$H = \Delta_s a_0^\dagger a_0 + \sum_{n=1}^{N} -Ka_n^{\dagger 2}a_n^2 + \Omega_p\left(a_n^{\dagger 2} + a_n^2\right) + \left[Ja_n a_0^\dagger \exp(i\Delta t) + \text{h.c.}\right]. \tag{D2}$$

Note that $\Delta_a > \Delta$ is tunable by changing the external magnetic flux according to Eq. (C7). For $t < \tau$, we assume Δ_a is so large that $\Delta_s \to 0$. At time $t = \tau_m$, we decrease the detuning Δ_a by changing the external magnetic flux for the auxiliary transmon qubit. Then, the detuning between each KPO mode a_n and the cavity mode a_0 becomes $\Delta' = \Delta + \Delta_s$. This approach has been widely used in quantum measurements, e.g., for the readout of final states.

ACKNOWLEDGMENTS

Y.-H.C. was supported by the Japan Society for the Promotion of Science (JSPS) KAKENHI Grant No. JP19F19028. W.Q. was supported in part by the Incentive Research Project of RIKEN. A.M. was supported by the Polish National Science Centre (NCN) under the Maestro Grant No. DEC-2019/34/A/ST2/00081. F.N. was supported in part by: Nippon Telegraph and Telephone Corporation (NTT) Research, the Japan Science and Technology Agency (JST) [via the Quantum Leap Flagship Program (Q-LEAP), and the Moonshot R&D Grant No. JPMJMS2061], the Japan Society for the Promotion of Science (JSPS) [via the Grants-in-Aid for Scientific Research (KAKENHI) Grant No. JP20H00134], the Army Research Office (ARO) (Grant No. W911NF-18-1-0358), the Asian Office of Aerospace Research and Development (AOARD) (via Grant No. FA2386-20-1-4069), and the Foundational Questions Institute Fund (FQXi) via Grant No. FQXi-IAF19-06.

[1] J. D. Hidary, *Quantum Computing: An Applied Approach* (Springer, Berlin, 2019).
[2] R. J. Lipton and K. W. Regan, *Introduction to Quantum Algorithms via Linear Algebra* (The MIT Press, Cambridge, 2021).
[3] M. A. Nielsen and I. L. Chuang, *Quantum Computation and Quantum Information* (Cambridge Univ. Press, Cambridge, 2000).
[4] A. F. Kockum and F. Nori, "Quantum bits with Josephson junctions," in *Fundamentals and Frontiers of the Josephson Effect*, Vol. 286, edited by F. Tafuri (Springer, Berlin, 2019) Chap. 17, pp. 703–741.
[5] M. Kjaergaard, M. E. Schwartz, J. Braumüller, P. Krantz, J. I.-J. Wang, S. Gustavsson, and W. D.

Oliver, "Superconducting qubits: Current state of play," Ann. Rev. Cond. Matt. Phys. **11**, 369–395 (2020).
[6] F. Arute, K. Arya, R. Babbush, D. Bacon, J. C. Bardin, R. Barends, R. Biswas, S. Boixo, F. G. S. L. Brandao, D. A. Buell, *et al.*, "Quantum supremacy using a programmable superconducting processor," Nature (London) **574**, 505–510 (2019).
[7] H.-S. Zhong, H. Wang, Y.-H. Deng, M.-C. Chen, L.-C. Peng, Y.-H. Luo, J. Qin, D. Wu, X. Ding, Y. Hu, *et al.*, "Quantum computational advantage using photons," Science **370**, 1460–1463 (2020).
[8] P. W. Shor, "Scheme for reducing decoherence in quantum computer memory," Phys. Rev. A **52**, R2493–R2496 (1995).
[9] A. Steane, "Multiple-particle interference and quantum error correction," Proc. Roy. Soc. Lond. A **452**, 2551–2577 (1996).
[10] A. Y. Kitaev, "Fault-tolerant quantum computation by anyons," Ann. Phys. **303**, 2–30 (2003).
[11] D. Gottesman, A. Kitaev, and J. Preskill, "Encoding a qubit in an oscillator," Phys. Rev. A **64**, 012310 (2001).
[12] M. Mirrahimi, Z. Leghtas, V. V. Albert, S. Touzard, R. J. Schoelkopf, L. Jiang, and M. H. Devoret, "Dynamically protected cat-qubits: a new paradigm for universal quantum computation," New J. Phys. **16**, 045014 (2014).
[13] M. Mirrahimi, "Cat-qubits for quantum computation," Comptes Rendus Phys. **17**, 778–787 (2016).
[14] C. Chamberland, K. Noh, P. Arrangoiz-Arriola, E. T. Campbell, C. T. Hann, J. Iverson, H. Putterman, T. C. Bohdanowicz, S. T. Flammia, A. Keller, G. Refael, J. Preskill, L. Jiang, A. H. Safavi-Naeini, O. Painter, and F. G. S. L. Brandão, "Building a fault-tolerant quantum computer using concatenated cat codes," PRX Quantum **3**, 010329 (2022).
[15] W. Cai, Y. Ma, W. Wang, C.-L. Zou, and L. Sun, "Bosonic quantum error correction codes in superconducting quantum circuits," Fund. Res. **1**, 50–67 (2021).
[16] W.-L. Ma, S. Puri, R. J. Schoelkopf, M. H. Devoret, S. M. Girvin, and L. Jiang, "Quantum control of bosonic modes with superconducting circuits," Sci. Bull. **66**, 1789–1805 (2021).
[17] T. C. Ralph, A. Gilchrist, G. J. Milburn, W. J. Munro, and S. Glancy, "Quantum computation with optical coherent states," Phys. Rev. A **68**, 042319 (2003).
[18] A. Gilchrist, K. Nemoto, W. J. Munro, T. C. Ralph, S. Glancy, S. L. Braunstein, and G. J. Milburn, "Schrödinger cats and their power for quantum information processing," J. Opt. B **6**, S828–S833 (2004).
[19] F. Gaitan, *Quantum Error Correction and Fault Tolerant Quantum Computing* (CRC Press, Boca Raton, 2008).
[20] D. A. Lidar and T. A. Brun, eds., *Quantum Error Correction* (Cambridge Univ. Press, New York, 2013).
[21] D. Gottesman, "An introduction to quantum error correction and fault-tolerant quantum computation," in *Quantum Information Science and Its Contributions to Mathematics, Proceedings of Symposia in Applied Mathematics*, Vol. 68 (American Mathematical Society, Washington, DC, 2010) Chap. 3, pp. 13–58.
[22] A. G. Fowler, M. Mariantoni, J. M. Martinis, and A. N. Cleland, "Surface codes: Towards practical large-scale quantum computation," Phys. Rev. A **86**, 032324 (2012).
[23] S. J. Devitt, W. J. Munro, and K. Nemoto, "Quantum error correction for beginners," Rep. Prog. Phys. **76**, 076001 (2013).
[24] J. Zhang, S. J. Devitt, J. Q. You, and F. Nori, "Holonomic surface codes for fault-tolerant quantum computation," Phys. Rev. A **97**, 022335 (2018).
[25] S. Puri, A. Grimm, P. Campagne-Ibarcq, A. Eickbusch, K. Noh, G. Roberts, L. Jiang, M. Mirrahimi, M. H. Devoret, and S. M. Girvin, "Stabilized cat in a driven nonlinear cavity: A fault-tolerant error syndrome detector," Phys. Rev. X **9**, 041009 (2019).
[26] D. Litinski, "A game of surface codes: Large-scale quantum computing with lattice surgery," Quantum **3**, 128 (2019).
[27] V. V. Albert, C. Shu, S. Krastanov, C. Shen, R.-B. Liu, Z.-B. Yang, R. J. Schoelkopf, M. Mirrahimi, M. H. Devoret, and L. Jiang, "Holonomic quantum control with continuous variable systems," Phys. Rev. Lett. **116**, 140502 (2016).
[28] M. H. Michael, M. Silveri, R. T. Brierley, V. V. Albert, J. Salmilehto, L. Jiang, and S. M. Girvin, "New class of quantum error-correcting codes for a bosonic mode," Phys. Rev. X **6**, 031006 (2016).
[29] R. W. Heeres, P. Reinhold, N. Ofek, L. Frunzio, L. Jiang, M. H. Devoret, and R. J. Schoelkopf, "Implementing a universal gate set on a logical qubit encoded in an oscillator," Nat. Commun. **8**, 94 (2017).
[30] L. Li, C.-L. Zou, V. V. Albert, S. Muralidharan, S. M. Girvin, and L. Jiang, "Cat codes with optimal decoherence suppression for a lossy bosonic channel," Phys. Rev. Lett. **119**, 030502 (2017).
[31] K. S. Chou, J. Z. Blumoff, C. S. Wang, P. C. Reinhold, C. J. Axline, Y. Y. Gao, L. Frunzio, M. H. Devoret, L. Jiang, and R. J. Schoelkopf, "Deterministic teleportation of a quantum gate between two logical qubits," Nature (London) **561**, 368–373 (2018).
[32] S. Rosenblum, Y. Y. Gao, P. Reinhold, C. Wang, C. J. Axline, L. Frunzio, S. M. Girvin, L. Jiang, M. Mirrahimi, M. H. Devoret, and R. J. Schoelkopf, "A CNOT gate between multiphoton qubits encoded in two cavities," Nat. Commun. **9**, 652 (2018).
[33] V. V. Albert, S. O. Mundhada, A. Grimm, S. Touzard., M. H. Devoret, and L. Jiang, "Pair-cat codes: autonomous error-correction with low-order nonlinearity," Quantum Sci. Tech. **4**, 035007 (2019).
[34] Y. Xu, Y. Ma, W. Cai, X. Mu, W. Dai, W. Wang, L. Hu, X. Li, J. Han, H. Wang, Y. P. Song, Z.-B. Yang, S.-B. Zheng, and L. Sun, "Demonstration of controlled-phase gates between two error-correctable photonic qubits," Phys. Rev. Lett. **124**, 120501 (2020).
[35] J. M. Gertler, B. Baker, J. Li, S. Shirol, J. Koch, and C. Wang, "Protecting a bosonic qubit with autonomous quantum error correction," Nature (London) **590**, 243–248 (2021).
[36] V. V. Dodonov, I. A. Malkin, and V. I. Man'ko, "Even and odd coherent states and excitations of a singular oscillator," Physica **72**, 597–615 (1974).
[37] Y.-x. Liu, L. F. Wei, and F. Nori, "Preparation of macroscopic quantum superposition states of a cavity field via coupling to a superconducting charge qubit," Phys. Rev. A **71**, 063820 (2005).
[38] M. Kira, S. W. Koch, R. P. Smith, A. E. Hunter, and S. T. Cundiff, "Quantum spectroscopy with

Schrödinger-cat states," Nat. Phys. **7**, 799–804 (2011).
[39] J. Gribbin, *Computing with Quantum Cats: From Colossus to Qubits* (Bantam Press, London, 2013).
[40] Z. Leghtas, S. Touzard, I. M. Pop, A. Kou, B. Vlastakis, A. Petrenko, K. M. Sliwa, A. Narla, S. Shankar, M. J. Hatridge, M. Reagor, L. Frunzio, R. J. Schoelkopf, M. Mirrahimi, and M. H. Devoret, "Confining the state of light to a quantum manifold by engineered two-photon loss," Science **347**, 853–857 (2015).
[41] Y.-H. Chen, W. Qin, X. Wang, A. Miranowicz, and F. Nori, "Shortcuts to adiabaticity for the quantum Rabi model: Efficient generation of giant entangled cat states via parametric amplification," Phys. Rev. Lett. **126**, 023602 (2021).
[42] Y.-H. Chen, W. Qin, R. Stassi, X. Wang, and F. Nori, "Fast binomial-code holonomic quantum computation with ultrastrong light-matter coupling," Phys. Rev. Res. **3**, 033275 (2021).
[43] R. Stassi, M. Cirio, K. Funo, N. Lambert, J. Puebla, and F. Nori, "Unveiling and veiling a Schrödinger cat state from the vacuum," arXiv:2110.02674 (2021).
[44] J. Guillaud and M. Mirrahimi, "Repetition cat qubits for fault-tolerant quantum computation," Phys. Rev. X **9**, 041053 (2019).
[45] A. Sørensen and K. Mølmer, "Quantum computation with ions in thermal motion," Phys. Rev. Lett. **82**, 1971–1974 (1999).
[46] A. Sørensen and K. Mølmer, "Entanglement and quantum computation with ions in thermal motion," Phys. Rev. A **62**, 022311 (2000).
[47] K. Mølmer and A. Sørensen, "Multiparticle entanglement of hot trapped ions," Phys. Rev. Lett. **82**, 1835–1838 (1999).
[48] P. Solinas, P. Zanardi, and N. Zanghì, "Robustness of non-Abelian holonomic quantum gates against parametric noise," Phys. Rev. A **70**, 042316 (2004).
[49] S.-L. Zhu and P. Zanardi, "Geometric quantum gates that are robust against stochastic control errors," Phys. Rev. A **72**, 020301(R) (2005).
[50] S.-B. Zheng, "Unconventional geometric quantum phase gates with a cavity QED system," Phys. Rev. A **70**, 052320 (2004).
[51] S.-B. Zheng, C.-P. Yang, and F. Nori, "Comparison of the sensitivity to systematic errors between nonadiabatic non-Abelian geometric gates and their dynamical counterparts," Phys. Rev. A **93**, 032313 (2016).
[52] C. Song, S.-B. Zheng, P. Zhang, K. Xu, L. Zhang, Q. Guo, W. Liu, D. Xu, H. Deng, K. Huang, D. Zheng, X. Zhu, and H. Wang, "Continuous-variable geometric phase and its manipulation for quantum computation in a superconducting circuit," Nat. Commun. **8**, 1061 (2017).
[53] Z.-Y. Xue, F.-L. Gu, Z.-P. Hong, Z.-H. Yang, D.-W. Zhang, Y. Hu, and J. Q. You, "Nonadiabatic holonomic quantum computation with dressed-state qubits," Phys. Rev. Appl. **7**, 054022 (2017).
[54] Y.-H. Kang, Y.-H. Chen, Z.-C. Shi, B.-H. Huang, J. Song, and Y. Xia, "Nonadiabatic holonomic quantum computation using Rydberg blockade," Phys. Rev. A **97**, 042336 (2018).
[55] L. K. Grover, "Quantum mechanics helps in searching for a needle in a haystack," Phys. Rev. Lett. **79**, 325–328 (1997).
[56] K.-A. Brickman, P. C. Haljan, P. J. Lee, M. Acton, L. Deslauriers, and C. Monroe, "Implementation of Grover's quantum search algorithm in a scalable system," Phys. Rev. A **72**, 050306(R) (2005).
[57] P. C. Haljan, K.-A. Brickman, L. Deslauriers, P. J. Lee, and C. Monroe, "Spin-dependent forces on trapped ions for phase-stable quantum gates and entangled states of spin and motion," Phys. Rev. Lett. **94**, 153602 (2005).
[58] G. Kirchmair, J. Benhelm, F. Zähringer, R. Gerritsma, C. F. Roos, and R. Blatt, "Deterministic entanglement of ions in thermal states of motion," New J. Phys. **11**, 023002 (2009).
[59] D. Hayes, S. M. Clark, S. Debnath, D. Hucul, I. V. Inlek, K. W. Lee, Q. Quraishi, and C. Monroe, "Coherent error suppression in multiqubit entangling gates," Phys. Rev. Lett. **109**, 020503 (2012).
[60] A. Lemmer, A. Bermudez, and M. B. Plenio, "Driven geometric phase gates with trapped ions," New J. Phys. **15**, 083001 (2013).
[61] F. Haddadfarshi and F. Mintert, "High fidelity quantum gates of trapped ions in the presence of motional heating," New J. Phys. **18**, 123007 (2016).
[62] H. Takahashi, P. Nevado, and M. Keller, "Mølmer-Sørensen entangling gate for cavity QED systems," J. Phys. B **50**, 195501 (2017).
[63] Y. Shapira, R. Shaniv, T. Manovitz, N. Akerman, and R. Ozeri, "Robust entanglement gates for trapped-ion qubits," Phys. Rev. Lett. **121**, 180502 (2018).
[64] T. Manovitz, A. Rotem, R. Shaniv, I. Cohen, Y. Shapira, N. Akerman, A. Retzker, and R. Ozeri, "Fast dynamical decoupling of the Mølmer-Sørensen entangling gate," Phys. Rev. Lett. **119**, 220505 (2017).
[65] A. Mitra, M. J. Martin, G. W. Biedermann, A. M. Marino, P. M. Poggi, and I. H. Deutsch, "Robust Mølmer-Sørensen gate for neutral atoms using rapid adiabatic Rydberg dressing," Phys. Rev. A **101**, 030301(R) (2020).
[66] Y. Wang, J.-L. Wu, J.-X. Han, Y.-Y. Jiang, Y. Xia, and J. Song, "Resilient Mølmer-Sørensen gate with cavity QED," Phys. Lett. A **388**, 127033 (2021).
[67] H. Haffner, C. Roos, and R. Blatt, "Quantum computing with trapped ions," Phys. Rep. **469**, 155–203 (2008).
[68] C. D. Bruzewicz, J. Chiaverini, R. McConnell, and J. M. Sage, "Trapped-ion quantum computing: Progress and challenges," Appl. Phys. Rev. **6**, 021314 (2019).
[69] P. Parrado-Rodríguez, C. Ryan-Anderson, A. Bermudez, and M. Müller, "Crosstalk suppression for fault-tolerant quantum error correction with trapped ions," Quantum **5**, 487 (2021).
[70] S. Puri, L. St-Jean, J. A. Gross, A. Grimm, N. E. Frattini, P. S. Iyer, A. Krishna, S. Touzard, L. Jiang, A. Blais, S. T. Flammia, and S. M. Girvin, "Bias-preserving gates with stabilized cat qubits," Sci. Adv. **6**, eaay5901 (2020).
[71] S. Puri, S. Boutin, and A. Blais, "Engineering the quantum states of light in a Kerr-nonlinear resonator by two-photon driving," npj Quantum Inf. **3**, 18 (2017).
[72] A. Miranowicz, J. Bajer, N. Lambert, Y.-x. Liu, and F. Nori, "Tunable multiphonon blockade in coupled nanomechanical resonators," Phys. Rev. A **93**, 013808 (2016).
[73] J. Bourassa, F. Beaudoin, Jay M. Gambetta, and A. Blais, "Josephson-junction-embedded transmission-line resonators: From Kerr medium

to in-line transmon," Phys. Rev. A **86**, 013814 (2012).
[74] A. Grimm, N. E. Frattini, S. Puri, S. O. Mundhada, S. Touzard, M. Mirrahimi, S. M. Girvin, S. Shankar, and M. H. Devoret, "Stabilization and operation of a Kerr-cat qubit," Nature (London) **584**, 205–209 (2020).
[75] N. A. Masluk, I. M. Pop, A. Kamal, Z. K. Minev, and M. H. Devoret, "Microwave characterization of Josephson junction arrays: Implementing a low loss superinductance," Phys. Rev. Lett. **109**, 137002 (2012).
[76] I. M. Pop, K. Geerlings, G. Catelani, R. J. Schoelkopf, L. I. Glazman, and M. H. Devoret, "Coherent suppression of electromagnetic dissipation due to superconducting quasiparticles," Nature (London) **508**, 369–372 (2014).
[77] J. Cohen, W. C. Smith, M. H. Devoret, and M. Mirrahimi, "Degeneracy-preserving quantum nondemolition measurement of parity-type observables for cat qubits," Phys. Rev. Lett. **119**, 060503 (2017).
[78] L. DiCarlo, J. M. Chow, J. M. Gambetta, L. S. Bishop, B. R. Johnson, D. I. Schuster, J. Majer, A. Blais, L. Frunzio, S. M. Girvin, and R. J. Schoelkopf, "Demonstration of two-qubit algorithms with a superconducting quantum processor," Nature (London) **460**, 240–244 (2009).
[79] J. R. Johansson, P. D. Nation, and F. Nori, "QuTiP: An open-source Python framework for the dynamics of open quantum systems," Comp. Phys. Comm. **183**, 1760 (2012).
[80] J. R. Johansson, P. D. Nation, and F. Nori, "QuTiP 2: A Python framework for the dynamics of open quantum systems," Comp. Phys. Comm. **184**, 1234–1240 (2013).
[81] Z. Wang, M. Pechal, E. A. Wollack, P. Arrangoiz-Arriola, M. Gao, N. R. Lee, and A. H. Safavi-Naeini, "Quantum dynamics of a few-photon parametric oscillator," Phys. Rev. X **9**, 021049 (2019).
[82] P. Zanardi and D. A. Lidar, "Purity and state fidelity of quantum channels," Phys. Rev. A **70**, 012315 (2004).
[83] L. H. Pedersen, N. M. Møller, and K. Mølmer, "Fidelity of quantum operations," Phys. Lett. A **367**, 47–51 (2007).
[84] S. Touzard, A. Kou, N. E. Frattini, V. V. Sivak, S. Puri, A. Grimm, L. Frunzio, S. Shankar, and M. H. Devoret, "Gated conditional displacement readout of superconducting qubits," Phys. Rev. Lett. **122**, 080502 (2019).
[85] Y. Y. Gao, B. J. Lester, Y. Zhang, C. Wang, S. Rosenblum, L. Frunzio, L. Jiang, S. M. Girvin, and R. J. Schoelkopf, "Programmable interference between two microwave quantum memories," Phys. Rev. X **8**, 021073 (2018).
[86] M. O. Scully and M. S. Zubairy, *Quantum Optics* (Cambridge University Press, Cambridge, England, 1997).
[87] Girish S. Agarwal, *Quantum Optics* (Cambridge University Press, Cambridge, England, 2012).
[88] L. Hu, Y. Ma, W. Cai, X. Mu, Y. Xu, W. Wang, Y. Wu, H. Wang, Y. P. Song, C.-L. Zou, S. M. Girvin, L.-M. Duan, and L. Sun, "Quantum error correction and universal gate set operation on a binomial bosonic logical qubit," Nat. Phys. **15**, 503–508 (2019).
[89] Y. Y. Gao, B. J. Lester, K. S. Chou, L. Frunzio, M. H. Devoret, L. Jiang, S. M. Girvin, and R. J. Schoelkopf, "Entanglement of bosonic modes through an engineered exchange interaction," Nature **566**, 509–512 (2019).
[90] J. Koch, T. M. Yu, J. Gambetta, A. A. Houck, D. I. Schuster, J. Majer, A. Blais, M. H. Devoret, S. M. Girvin, and R. J. Schoelkopf, "Charge-insensitive qubit design derived from the cooper pair box," Phys. Rev. A **76**, 042319 (2007).
[91] J. Q. You, X. Hu, S. Ashhab, and F. Nori, "Low-decoherence flux qubit," Phys. Rev. B **75**, 140515(R) (2007).
[92] E. Flurin, N. Roch, J. D. Pillet, F. Mallet, and B. Huard, "Superconducting quantum node for entanglement and storage of microwave radiation," Phys. Rev. Lett. **114**, 090503 (2015).
[93] W. Wustmann and V. Shumeiko, "Parametric resonance in tunable superconducting cavities," Phys. Rev. B **87**, 184501 (2013).
[94] X. Gu, A. F. Kockum, A. Miranowicz, Y. x. Liu, and F. Nori, "Microwave photonics with superconducting quantum circuits," Phys. Rep. **718-719**, 1–102 (2017).
[95] P. Krantz, M. Kjaergaard, F. Yan, T. P. Orlando, S. Gustavsson, and W. D. Oliver, "A quantum engineer's guide to superconducting qubits," Appl. Phys. Rev. **6**, 021318 (2019).
[96] S. Kwon, A. Tomonaga, G. L. Bhai, S. J. Devitt, and J.-S. Tsai, "Gate-based superconducting quantum computing," J. Appl. Phys. **129**, 041102 (2021).
[97] P. D. Nation, J. R. Johansson, M. P. Blencowe, and F. Nori, "Colloquium: Stimulating uncertainty: Amplifying the quantum vacuum with superconducting circuits," Rev. Mod. Phys. **84**, 1–24 (2012).
[98] M. Wallquist, V. S. Shumeiko, and G. Wendin, "Selective coupling of superconducting charge qubits mediated by a tunable stripline cavity," Phys. Rev. B **74**, 224506 (2006).
[99] J.-Q. Liao, Z. R. Gong, L. Zhou, Y.-x. Liu, C. P. Sun, and F. Nori, "Controlling the transport of single photons by tuning the frequency of either one or two cavities in an array of coupled cavities," Phys. Rev. A **81**, 042304 (2010).
[100] Z.-L. Xiang, S. Ashhab, J. Q. You, and F. Nori, "Hybrid quantum circuits: Superconducting circuits interacting with other quantum systems," Rev. Mod. Phys. **85**, 623–653 (2013).
[101] O. Yaakobi, L. Friedland, C. Macklin, and I. Siddiqi, "Parametric amplification in Josephson junction embedded transmission lines," Phys. Rev. B **87**, 144301 (2013).
[102] C. Macklin, K. O'Brien, D. Hover, M. E. Schwartz, V. Bolkhovsky, X. Zhang, W. D. Oliver, and I. Siddiqi, "A near-quantum-limited Josephson traveling-wave parametric amplifier," Science **350**, 307–310 (2015).
[103] A. Roy and M. Devoret, "Introduction to parametric amplification of quantum signals with Josephson circuits," Comptes Rendus Phys. **17**, 740–755 (2016).
[104] X. Wang, A. Miranowicz, and F. Nori, "Ideal quantum nondemolition readout of a flux qubit without Purcell limitations," Phys. Rev. Appl. **12**, 064037 (2019).
[105] S. Masuda, T. Ishikawa, Y. Matsuzaki, and S. Kawabata, "Controls of a superconducting quantum parametron under a strong pump field," Sci. Rep. **11** (2021).
[106] Y.-H. Chen, W. Qin, and F. Nori, "Fast and high-fidelity generation of steady-state entanglement using pulse modulation and parametric amplification," Phys. Rev. A **100**, 012339 (2019).

[107] W. Qin, V. Macrì, A. Miranowicz, S. Savasta, and F. Nori, "Emission of photon pairs by mechanical stimulation of the squeezed vacuum," Phys. Rev. A **100**, 062501 (2019).

[108] W. Qin, Y.-H. Chen, X. Wang, A. Miranowicz, and F. Nori, "Strong spin squeezing induced by weak squeezing of light inside a cavity," Nanophotonics **9**, 4853–4868 (2020).

[109] W. Qin, A. Miranowicz, H. Jing, and F. Nori, "Generating long-lived macroscopically distinct superposition states in atomic ensembles," Phys. Rev. Lett. **127**, 093602 (2021).